Tunable Alkylation of White Graphene (Hexagonal-

Boron Nitride) using Reductive Conditions

Carlos A. de los Reyes, Katharyn Hernández, Cecilia Martínez-Jiménez, Kendahl L. Walz Mitra, Cedric Ginestra, Ashleigh D. Smith McWilliams, Matteo Pasquali, Ashleigh A. Martí*, $\mathbb{R}^{\mathbb{R}, \mathbb{R}, \mathbb{R}, \mathbb{R}}$

Departments of Chemistry,[¶] Chemical and Biomolecular Engineering,[§] Materials Science and NanoEngineering,[‡] Bioengineering,[‡] and Smalley-Curl Institute for Nanoscale Science and Technology,[∞] Rice University, Houston Texas 77005, United States.

ABSTRACT. Hexagonal boron nitride (h-BN), also known as white graphene, presents an unparalleled combination of properties, including superior mechanical strength, good thermal conductivity, a wide band gap, and chemical and thermal inertness. However, because of its aversion to chemical modification, its applications have not progressed as much as those of carbon nanomaterials. In this manuscript, we show the functionalization of hexagonal boron nitride using alkyl halides in strongly reducing conditions (Billups-Birch conditions). The tunability of the Billups-Birch reaction is demonstrated by alkylating hexagonal boron nitride with 1-bromododecane and varying equivalents of Li to BN. We found that using a 1:20 BN/Li ratio yields the highest chemical modification, as demonstrated using TGA, FTIR, and supported by XPS. Imaging of the functionalized h-BN (fh-BN) revealed that its sheets exfoliate better in isopropanol than pristine h-BN, which displays highly stacked nanostructures. Moreover, bearing

alkyl chains confers the nanosheets with improved dispersibility in non-polar solvents, such as dodecane, and allows the formation of hydrophobic films.

INTRODUCTION

Ever since the discovery of nanostructures such as graphene,¹ carbon nanotubes (CNTs),² and the fullerene,³ scientists have acknowledged their unique intrinsic properties given by the confinement of at least one of their dimensions. Much research has, therefore, been geared towards their understanding, manipulation, and modification. Notably, the ability to obtain monoatomic layered graphene from graphite revolutionized the nanotechnology field as this led to the attainment of new layered nanomaterials from bulk precursors, such as molybdenum disulfide,⁴ black phosphorus,⁵ hematite,⁶ and hexagonal boron nitride,⁷ to name a few.

From these layered materials, hexagonal boron nitride (h-BN) is remarkable due to its unique set of properties, which has given rise to a wide variety of potential applications. h-BN, also known as white graphene due to its white color, has a hexagonal structure similar to graphene, but carbon atoms are substituted for alternating boron and nitrogen. It has been reported that a boron nitride nanosheet (BNNS) presents a Young's modulus of 865 GPa,⁸ a value four times greater than that of steel. Additionally, the measured thermal conductivity was determined to be 600 W m⁻¹ K⁻¹ for a single layer.⁹ While this value decreases as the number of layers increases, only 11 sheets are needed to reach the value of bulk h-BN (360 W m⁻¹ K⁻¹), the value is comparable to that of copper (ca. 390 W m⁻¹ K⁻¹).¹⁰ Another outstanding property of h-BN is its wide band gap of 5.9 eV,¹¹ a characteristic not found in carbon nanomaterials. This property has been demonstrated to be useful in electronic¹²⁻¹³ and optical devices,^{11, 14} neutron capture,¹⁵⁻¹⁶ and sensing.¹⁷⁻¹⁸ Lastly, it is known that boron nitride nanomaterials have pronounced chemical and

thermal stability,¹⁹ making them desirable for the production of materials required to work in severe conditions. Given its mechanical and thermal properties, h-BN has been used as an additive for polymers²⁰⁻²² and oils.²³

Even though boron nitride nanomaterials have been explored in many areas and envisioned for more applications, the list of examples would be longer if some hurdles could be overcome. For instance, boron nitride nanomaterials are known to have low dispersibility in solvents, which is an important step to produce a functional macroscopic material. Secondly, their high chemical and thermal stability translate into an increased difficulty for their chemical modification, which is a necessary step to tune the properties of any nanomaterial. In this regard, the number of examples about the chemical modification of boron nitride nanomaterials is significantly lower than that of carbon nanomaterials.

There have been few examples of functionalization of boron nitride nanomaterials reported, and they can be categorized by their methodologies. For instance, sonication-assisted methods have been employed to introduce hydroxyl,²⁴ amino²⁵ and alkyl groups.²⁶ These involve long periods of sonication with the addend precursor used as the dispersing solvent. Other reported methods involve reactions in autoclaves, under high temperature and pressure, which induce the formation of radical species capable of attacking the boron atoms. This method was utilized to introduce hydroxyl groups from H₂O₂²⁷ and steam,²⁸ and to decorate with *tert*-butoxy groups using di-*tert*-butyl peroxide.²⁹ Plasma-assisted methods have been used, as well, to introduce functionalities from the atmosphere utilized during the process. For example, it has been reported that plasma produced from air generates hydroxyl groups,³⁰ while the utilization of ammonia plasma produces amino groups.³¹ Another type of methodology is ball milling, which has been

used to obtain hydroxyl³² and amino groups³³ on the boron nitride surface using sodium hydroxide and urea as reagents, respectively.

One kind of functionalization that has not been sufficiently explored for boron nitride nanomaterials is using reductive conditions. The reduction of nanomaterials has proven to be a powerful way to modify their properties, given that reduced species present enhanced reactivity towards a variety of molecules. This methodology has proven successful to functionalize carbon nanomaterials. For instance, alkali metal naphthalides have been used to covalently attach a variety of moieties to carbon nanotubes. 34-37 Similarly, sodium naphtalide in THF was used as the reductive solution functionalize boron nitride nanotubes (BNNTs) with 1-bromohexane. 38 It is also worth mentioning that graphite has been alkylated using this method, 39 yielding a material dispersible in organic solvents.

Another type of reductive condition used to functionalize carbon nanomaterials is the Billups-Birch reaction, which is faster and more straightforward than utilizing alkali metal naphtalides, as the reduction and addition of the addend occur *in situ*. The reaction relies on the utilization of an electride, in this case, ammonia molecules solvating electrons provided by an alkali metal, which can negatively charge the nanomaterial and react with any molecule capable of forming a radical. Because of its practicality, it has been used to decorate carbon nanomaterials with protons⁴⁰⁻⁴² and phenyl,⁴³ alkyl,⁴⁴⁻⁴⁷ alcohol, and ketone groups.⁴⁸ Additionally, fluorinated graphite was also alkylated using this reaction, enhancing their dispersibility in aprotic organic solvents.⁴⁹ Although this method has been used extensively for carbon, it has only recently found application in boron nitride functionalization. Our research group functionalized multi-walled boron nitride nanotubes with dodecyl chains using lithium, liquid ammonia, and 1-bromododecane as reagents.⁵⁰⁻⁵¹

Because of the importance of the Billups-Birch reaction as a versatile tool for the chemical modification of nanomaterials, it is crucial to gain further insight into this reaction as a means to functionalize boron nitride nanomaterials. Furthermore, even when this reaction has been successfully used for functionalizing BNNTs, it must be noted that BNNTs are expected to be more reactive that h-BN due to their intrinsic curvature, and therefore h-BN functionalization using the Billups-Birch reaction is not trivial. Hence, in this work we will study the functionalization of h-BN using Billups-Birch conditions. Using this reaction, we can tune the degree of functionalization of hexagonal boron nitride with alkyl chains by varying the amount of lithium, which is used as the electron source. Our results show that good control over the number of alkyl addends can be achieved, as demonstrated by thermogravimetric analysis and infrared spectroscopy. X-ray photoelectron spectroscopy was utilized to further verify covalent bonding between carbon and boron nitride. The dispersion of functionalized h-BN (fh-BN) was tested in different solvents and their ability to exfoliate was studied as well. Like in the case of graphite, upon alkylation, fh-BN disperses better in organic solvents than its precursor. Microscopy techniques, such as TEM and SEM, were used to analyze the structural integrity of fh-BN. Lastly, films of fh-BN were fabricated and their affinity to water was studied.

METHODS

Materials. Hexagonal boron nitride (1 μm in diameter), lithium and 1-bromododecane were purchased from Sigma Aldrich and anhydrous ammonia from Airgas. All solvents utilized were used fresh from the bottle and dodecane was purified by stirring it with concentrated sulfuric acid for 3 days and collected with a separation funnel.

Preparation of functionalized hexagonal boron nitride (fh-BN). In a typical experiment, ovendried hexagonal boron nitride powder (30 mg, 1.2 mmol) was added to an oven-dried and flamedried three-neck round bottom flask (250 mL) with varying amounts of lithium, according to a desired molar ratio. The system was purged three times with argon and then, with an acetone-dry ice bath, anhydrous ammonia was allowed to condense until it filled approximately one third of the containing vessel. Using a glass-coated magnetic stir bar, the reaction was stirred for an hour prior to the dropwise addition of 1-bromododecane (2.9 mL, 12.1 mmol). The mixture was then allowed to stir overnight at room temperature, which also permits the evaporation of ammonia. After the evaporation of ammonia, 40 mL of cold water-ethanol (3:1) was injected into the flask under inert atmosphere and an ice bath was used to avoid a vigorous reaction. 10% w/w HCl was added to the mixture until it reached an acidic pH in order to dissolve any lithium salts. The aqueous solution was extracted with n-hexanes, the interphase and organic phase were saved and filtered through a 0.4 µm PTFE membrane, and then were further washed with more n-hexanes and ethanol, in that order. Finally, the powder was allowed to dry at 120 °C under vacuum before any characterization. Different lithium to boron nitride molar ratios were used in order to produce fh-BN 1:5, 1:10, 1:20, 1:40, and 1:60, where, for example, 1:20 denotes 20 moles of lithium per mol of BN. Every ratio was produced in triplicate.

Control experiments. All BN/Li ratios were repeated using the same procedure just described without adding any alkyl halide. Additionally, a 1:0 ratio was prepared, where h-BN was only stirred in ammonia with the alkyl halide, but without the addition of lithium.

Preparation of dispersions. The materials were dispersed by bath sonication for 30 minutes in water, IPA, THF, or dodecane at a concentration of 0.25 mg/mL. Then, the dispersions were centrifuged at 9,000g for 30 minutes in centrifuge tubes lined with glass inserts to avoid plastic

contamination. The supernatants were extracted and submitted to a second round of centrifugation, again at 9,000g for 30 minutes. The scattering of the supernatant was evaluated with a Shimadzu UV 2450. Water, IPA and dodecane were evaluated at 255 nm. Due to the quantitative cutoff wavelength of THF, the scattering was measured at 285 nm. Then, in order to compare the values with the rest of the solvents, we obtained the 285/255 nm ratio of h-BN in water and applied such ratio to extrapolate the 285 nm value of THF to 255 nm. Each dispersion was prepared and measured in triplicate.

Instrumentation and analysis. FTIR spectra were obtained by averaging 64 scans using a Nicolet 6700 with ATR accessory and a resolution of 4 cm⁻¹. TGA was performed with a Q-600 Simultaneous TGA/DSC from TA instruments. The TGA program involved an isotherm at 115 °C for 20 min in order to remove water and then a ramp to 1000 °C at a rate of 10 °C/min. Argon was flowed at 80 ml/mL. To analyze the weight loss, the thermograms were normalized at 120 °C and the change in weight was measured at 900 °C. XPS measurements were carried out using a Phi Quantera scanning X-ray microprobe. 140 eV were used for the survey scans and 26 eV for the high-resolution analyses. To prepare the samples, dispersions in IPA were prepared (0.25 mg/mL; centrifugation at 9,000g) and drop-casted onto glass until a film was observed. Spectra were fitted with Multipak Software and shifted to the Si 2p peak centered at 1072.5 eV. AFM was performed with a Nanoscope IIIa scanning probe microscope controller from Digital Instruments; the samples were prepared from the same dispersion in IPA. TEM was performed with a JEOL 1230 high contrast transmission electron microscope operated at 80 kV. For analysis, the same dispersion described for XPS analysis was prepared and the supernatant casted on lacey carbon grid with a 400 µm mesh. SEM was performed on a FEI Quanta 400 ESEM operated at 5 kV. Samples were dispersed in IPA (0.25 mg/mL) and centrifuged at 1000g. The supernatant was drop-casted on a

silicon substrate and coated with 2 nm of gold. For high-resolution TEM, samples were prepared as for high-contrast TEM but the grids were submitted to vacuum drying (170 °C) for three nights and further argon-plasma cleaned for 10 seconds. High-resolution TEM was performed on a FEI Titan Themis³ S/TEM at an accelerating voltage of 300 kV.

Water-contact angle measurements. In order to produce films, h-BN or fh-BN were dispersed in 7 mL of IPA (0.5 mg/mL) and bath sonicated for 30 min. The suspensions were passed through a 11.0 μ m pore size, hydrophilic nylon membrane (47 mm in diameter) purchased from Millipore. The porous membrane allows the suspension to pass through with the assistance of vacuum. After, the filtrate was passed through the cake twice more. Finally, the membrane is washed with acetone and put to dry under vacuum at 110 °C for 2 hours. Photographs of the drops were obtained by depositing a 5 μ L drop of water on the material and recorded with a Ramé-hart contact angle goniometer (Model 100-01S) with a U1 series super speed digital camera and DROPimage Standard software. Water-contact angle analysis was conducted in ImageJ by using the sessile drop technique, which involves measuring the inner angle between the horizontal and a line tangential to the drop edge. The angle analysis was repeated on both sizes of the drop and averaged; 3 drops were measured for each

RESULTS AND DISCUSSION

Optimization of the degree of alkylation. As previously mentioned, one of the advantages of the Billups-Birch reaction for the functionalization of nanomaterials is its straightforwardness, as the reduction and addend-grafting steps occur *in situ*. In order to rationalize the reaction between

hexagonal boron nitride and 1-bromododecane (C₁₂H₂₅Br) that we present here, it is essential to look at the functionalization of carbon nanotubes. The mechanism for this reaction with carbon nanotubes was proposed by Billups, ^{44,52} who suggested that the ammonia-solvated electrons provided by lithium atoms reduce the CNTs to form negatively charged tubes. After that, these CNT salts can induce the formation of a transient radical anion of the alkyl halide through a single electron transfer mechanism. The dissociation of the alkyl halide follows the formation of a temporary radical anion producing the respective halide and a carbon-centered free radical that can readily attack the nanotubes. For h-BN, upon formation of the carbon free radical, boron atoms bearing excess electrons are able to form a covalent bond reacting with the alkyl radical.³⁸ This must be particularly relevant in defect sites, where reduction of boron sites would be easier.

In the present study, we performed a series of reactions between h-BN and $C_{12}H_{25}Br$ using lithium as the alkali metal to form functionalized h-BN sheets (fh-BN). We varied the amount of lithium utilized while fixing the equivalents of $C_{12}H_{25}Br$. We also performed control experiments using the same ratios of BN/Li without the addition of 1-bromododecane. Additionally, the control denoted as 1:0 was only stirred with $C_{25}H_{25}Br$ in ammonia. A summary of the reactions is presented in Figure 1.

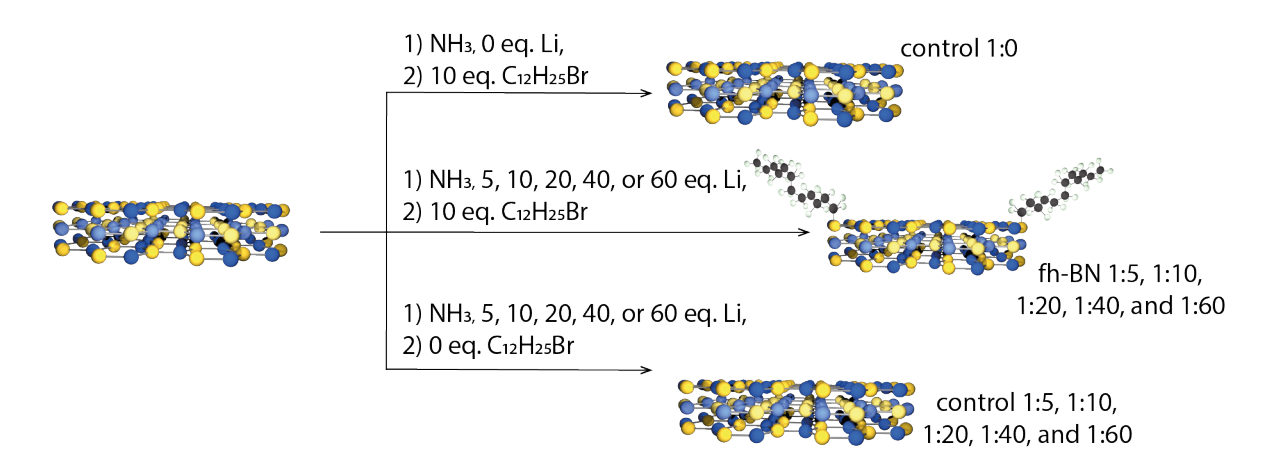


Figure 1. Experimental design to optimize the degree of functionalization of h-BN and produce functionalized hexagonal boron nitride (fh-BN).

In order to determine the efficiency of all reactions, we utilized infrared spectroscopy (FTIR) and thermogravimetric analysis (TGA), performed in an inert atmosphere, as the first means of characterization. While FTIR should reveal a set of C-H_{st} vibrations between 2800 and 3000 cm⁻¹, originated from the alkyl chains, TGA should show a weight loss due to desorption of addends. Figure S1 presents the FTIR spectra of pristine h-BN, fh-BN 1:20, and the spectrum of 1-bromododecane. Both h-BN and fh-BN 1:20 possess the typical vibrations attributed to this nanomaterial, which are the B-N stretching along the plane (B-N_{st}) at 1380 cm⁻¹ and the B-N out-of-plane bending (B-N_{bend}) at 765 cm⁻¹.⁵³ Unlike h-BN, fh-BN 1:20 presents the C-H_{st} vibrations that match those of 1-bromododecane. To further analyze these vibrations in al samples, in Figure 2a we present the FTIR spectra of pristine h-BN, control 1:0, and all the functionalization ratios tested, as well as, the spectrum of 1-bromododecane. It is noticeable that samples exposed to the Billups-Birch reaction conditions seem to experience slight shifts in the B-N stretching energy that may be due to lattice deformation³⁸ and has been previously observed upon functionalizing

BNNTs. $^{50-51}$. The inset in Figure 2a shows an enlargement of the C-H_{st} region , and it is qualitatively discernible that the intensity of these peaks increases from 1:5 to 1:20, and then decreases in 1:40 and even more in 1:60. We further analyzed the infrared spectra by obtaining the ratio between the most intense peak of CH_{st} vibrations (2920 cm⁻¹) and the B-N_{st} (Figure 2b). The results obtained from the triplicate of each reaction show that, indeed, this ratio increases going from h-BN to fh-BN 1:20 and then decreases with further addition of lithium. Moreover, the intensity of the C-H_{st} in fh-BN 1:20 is statistically significantly more intense than the rest of the samples. Finally, the controls 1:5 to 1:60 do not show any alkyl vibration, given that they were not in contact with $C_{12}H_{25}Br$ at any point, but also demonstrating that organic solvents involved in the work-up do not appear in the FTIR spectra.

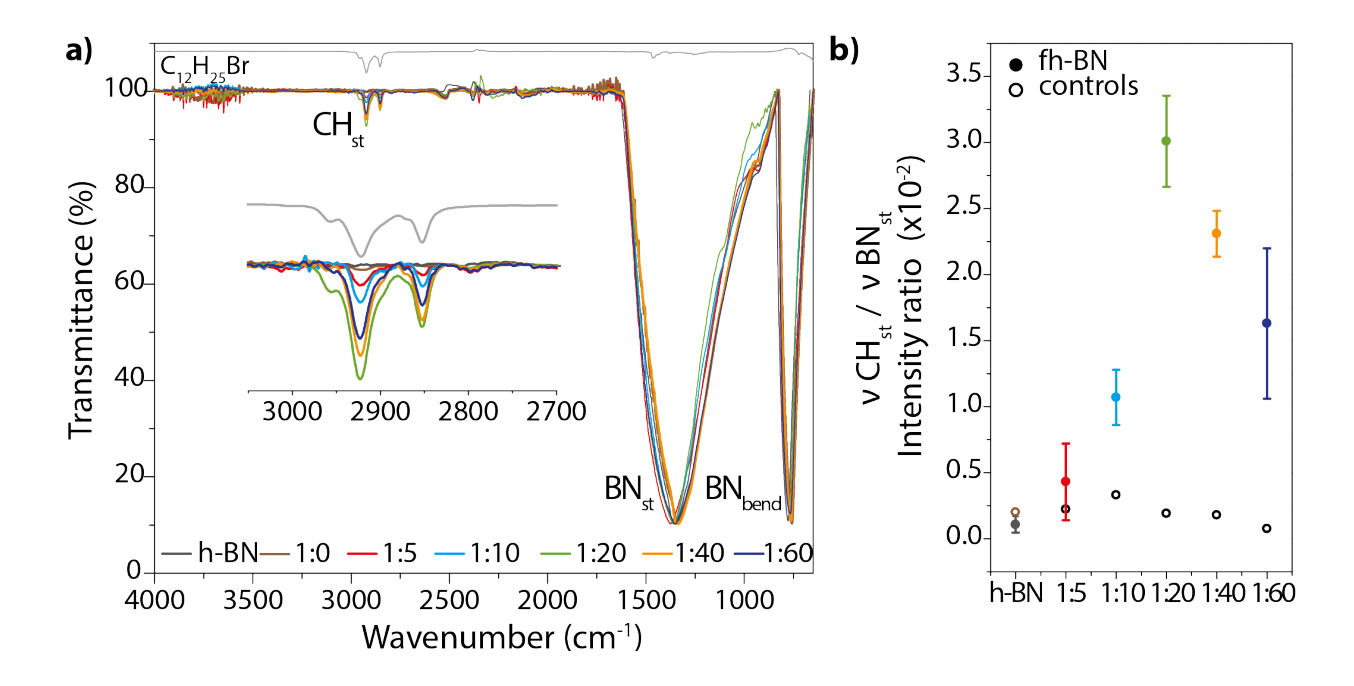


Figure 2. (a) Infrared spectra of h-BN, control 1:0, and fh-BN 1:(5-60) with an enlargement of the C-H_{st} vibrations. (b) Ratio between the CH_{st} and B-N_{st} vibrations as a function of BN/Li ratio. The

largest intensity of CH_{st} vibration to B-N_{st} vibration is found when increasing from 1:5 to a 1:20 BN/Li ratio and then it decreases again.

The TGA under argon revealed that while h-BN did not lose noticeable weight, all other samples show a weight loss spanning from ca. 200 °C to 500 °C (Figure 3a); however, the extent of their weight loss is quite different. The fh-BN 1:0 shows weight loss that must come from desorption of solvents, as this sample does not reveal any sign of alkyl chains in the FTIR. The weight loss values become increasingly larger as we go from 1:5 to 1:20 and then decrease again until we reach the 1:60 ratio, the same trend observed with FTIR. By producing each sample in triplicate, we could also observe that fh-BN 1:20 experiences a more statistically significant weight loss than the other samples, further corroborating the trend observed with the CH_{st}/BN_{st} ratio (Figure 3b). Moreover, from the control experiments we can conclude that the work-up process does not contribute much weight loss to the analysis. Nevertheless, we considered the weight loss experienced by the control experiments as inherent to this reaction, and, thus, we subtracted each value from its respective functionalized sample. Finally, from the average weight loss values, we can deduce the number of dodecyl chains present in each fh-BN sample. We determined that for fh-BN 1:20 there is ca. one alkyl chain per 60 BN units. The data from FTIR and TGA is summarized in Table 1.

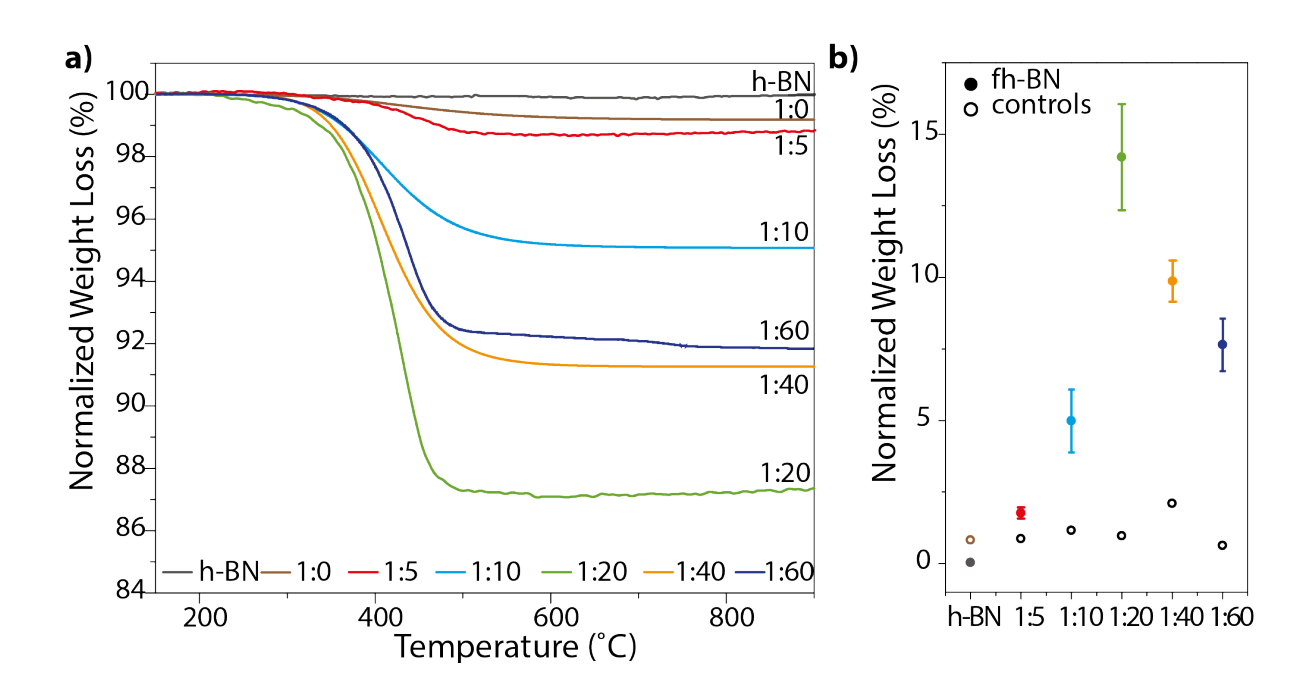


Figure 3. (a) Weight loss experienced under argon atmosphere for h-BN and all fh-BN samples. (b) Weight loss as a function of BN/Li ratio. The largest weight loss (correlated to highest degree of functionalization) is found when increasing from 1:5 to a 1:20 BN/Li ratio and then it decreases again.

Table 1. Summary of the CH_{st}/BN_{st} vibrations ratio obtained from the infrared spectra and the weight loss observed in the thermograms. The BN units per chain were calculated taking into account the weight loss of the control experiments.

	CH_{st}/BN_{st} $(1x10^{-2})$	CH_{st}/BN_{st} control $(1x10^{-3})$	Weight loss	Weight loss control	BN units per chain
h-BN	$0.06 (\pm 0.02)$	0.20	$0.03 (\pm 0.05)$	0.82	_
fh-BN 1:5	$0.56 (\pm 0.05)$	0.33	$1.76~(\pm~0.19)$	0.86	734
fh-BN 1:10	0.98 (± 0.29)	0.22	4.98 (± 1.1)	1.15	168
fh-BN 1:20	2.75 (± 0.15)	0.10	11.01 (± 1.2)	0.97	60
fh-BN 1:40	2.37 (± 0.18)	0.19	$8.17 (\pm 0.59)$	2.1	102
fh-BN 1:60	$1.15 (\pm 0.41)$	0.00	$6.35~(\pm~0.75)$	0.63	111

Through the intensity of the C-H_{st} vibrations and TGA analyses, we show evidence of the unmistakable trend of increasing degree of functionalization going from 1:5 to 1:20 BN/Li ratio and then of its decrease until 1:60. We believe that this behavior can be explained by the occurrence of two competing processes. Ammonia, which is in excess, can also be reduced to form lithium amide (LiNH₂), as is known to take place with alkali metals in ammonia, ⁵⁴ and has been a reason of concern in the functionalization of SWCNTs using this methodology. ⁵⁵⁻⁵⁶ On the other hand, having an excess of lithium metal (and electrons) may propitiate the formation of excess alkyl radicals, even far from the BN sheets, leading to side reactions that do not include functionalization. Therefore, a certain amount of lithium is needed to overcome the formation of LiNH₂ and lead to the formation of alkyl radicals nearby the sheets, and thus it is expected that the reaction efficiency increases with the concentration of lithium, however, too much lithium will cause side reactions of the alkyl halide that will reduce the efficiency. We believe that at a 1:20 molar ratio of BN/Li these opposite reactions compensate each other to yield the highest functionalization.

We performed additional characterization of all the samples with X-ray photoelectron spectroscopy (XPS) by dispersing the material in IPA and drop-casting it on glass slides until a white film was visible. The atomic composition found in the survey scans (Figure S2) show B, N, C, O, and Si in all samples, where O and Si are from the glass slide. Additionally, a control experiment, where only IPA was drop-casted with approximately the same number of drops, shows only C, Si, and O. Given that h-BN and fh-BN 1:0 are not supposed to show carbon content, we performed high-resolution XPS on the B1s, N1s, and C1s peaks in order to tell apart adventitious carbon and carbon due to alkyl chains (Figure S3). In order to distinguish new contributions to the signals of each element, we fixed the binding energies (B.E.) and FWHM values obtained from h-

BN to all other samples; all calculated values are shown in Table S1. From the high resolution scans, we observe that all samples show the typical values of 190.8 - 190.7 eV in the B1s peak for the B-N binding energy and 398.3 - 398.4 eV in the N1s peak for the N-B binding energy. Additionally, all samples, including the pristine material, exhibit additional Gaussian components at ca. 192 eV and 399 eV in the B1s and N1s peaks, respectively, that have been previously assigned to oxides. Contrasting with the pristine h-BN and control 1:0, the remaining fh-BN samples present a third Gaussian component in the B1s peak at a lower energy that can be attributed to the B-C binding energy. Lastly, the C1s peak of all samples presents C-C (284.8 eV) and C-O (286.0 eV) components, but only those that underwent functionalization present a component at lower energy that we can attribute to C-B (284.0 eV).

Change in dispersion and exfoliation. All further studies were carried out with fh-BN 1:20, given that thermogravimetric and spectroscopic characterization suggests a higher degree of functionalization than the other samples. After performing functionalization on BNNTs in the past, we observed different dispersibility behavior to that of its precursor, 50 so we decided to conduct this kind of study on fh-BN. We dispersed h-BN and fh-BN 1:20 (0.25 mg/mL) in water, IPA, THF, and dodecane using bath sonication for 30 mins, followed by two rounds of centrifugation for 30 mins at 9,000g, where the supernatant was transferred between rounds. The results in Figure 4 show the absorbance values normalized to the value obtained for h-BN for each solvent. Figure S4 shows a representative UV-Vis spectrum for h-BN and fh-BN 1:20 measured in each solvent and Figure S5 the absolute absorbance values for the three measurements in each solvent. Right after sonication, the low affinity of fh-BN to water is observable as the dispersion is clear and the material lies on the meniscus or on the bottom of the vial, which is in considerable contrast with h-BN that makes a milky suspension in water. This also impacts the UV-Vis results, where the

value of fh-BN in water is roughly a third of that of h-BN. In IPA, the samples behaved in the same way, where the h-BN dispersions show larger absorbance values than the fh-BN dispersion. We decided to test THF, as it is useful when volatile solvents are required. It is hard to draw a conclusion for this solvent as the absorbance values are not significantly different. Lastly, the average absorbance value of fh-BN dispersed in dodecane is more than 5 times larger than that of h-BN. The enhanced dispersion of fh-BN in this solvent is in agreement with what we observed previously when we compared dodecyl-BNNTs and BNNTs.⁵⁰ We believe the alkyl chains in the modified nanosheets play an essential role in allowing them to be stable in this solvent, probably due to interactions between the grafted dodecyl chains and dodecane.

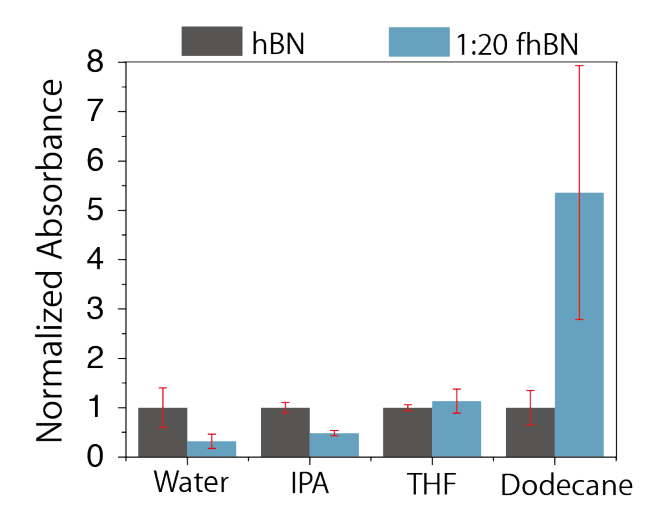


Figure 4. Dispersions of h-BN and fh-BN (1:20) in water, IPA, THF, and dodecane evaluated by UV-Visible spectroscopy.

To study the exfoliation of h-BN and fh-BN, we drop-casted IPA dispersions on mica (see experimental section for details) and studied them with AFM. A general observation in h-BN is that the images reveal a very clumped material (Figure 5a). This description is more evident when looking at the average height of 100 sheets, which spans from a few nanometers up to 40 nm (Figure 5b). In comparison, fh-BN sheets appear more defined, with heights that are ca. 1.2 nm on

average, corresponding to 3-4 layers considering a 3.33 Å spacing. The average diameter of the sheets is only slightly different, with somewhat larger sheets in fh-BN (Figure 5c).

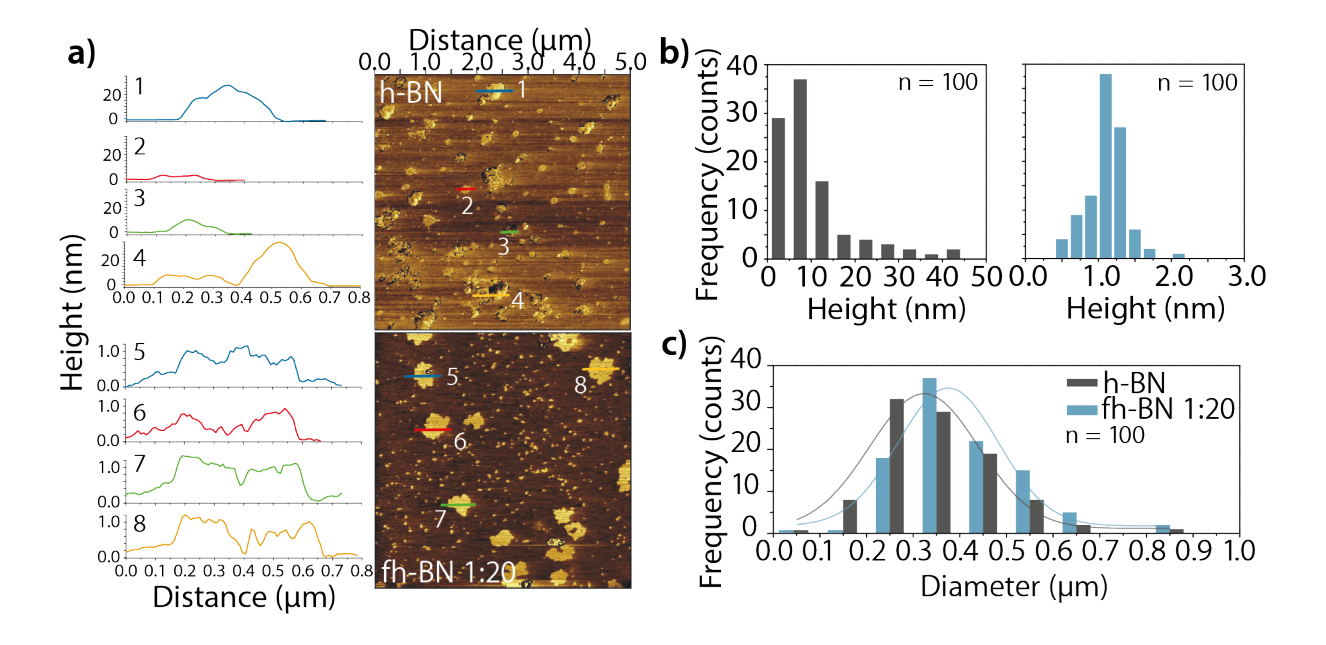


Figure 5. Atomic force microscopy characterization. (a) Representative AFM images of h-BN and fh-BN 1:20 with some height profiles. (b) Distribution of the heights of 100 sheets. (c) Distribution of the diameters of 100 sheets.

Structural characterization of h-BN and fh-BN 1:20. The sheets were structurally characterized with transmission electron microscopy (TEM, Figure 6) and scanning electron microscopy (SEM, Figure 7). When observed in the TEM, h-BN sheets appear as featureless structures with rounded edges (Figure 6a). It is difficult to determine the lateral dimensions of these sheets as they appear to be highly stacked. The stacking is even more evident if we look for the six-fold symmetry pattern characteristic of structure with hexagonal lattices using electron diffraction (ED).⁶⁰ ED patterns of h-BN were obtained where the red and blue dots are shown. The Figure 6c displays the ED of the dot closest to the edge, and it shows a few sets of dots with six-fold symmetry, characteristic of stacked structures.⁶¹ In contrast, another ED was taken in the center, and the diffracted spots form a diffuse halo, making more obvious the highly stacked structure with sheets in different

orientations (Figure 6d). fh-BN is different from h-BN in a few aspects (Figure 6b). First, the edges are sharper, as if they had been cut. Secondly, the sheets appear to fold. Bending or buckling has been observed to occur in few-layered boron nitride sheets⁶¹ and graphene, and has been ascribed to a mechanism of free surface energy, or as a result of elastic strain or dislocations.⁶⁰ In our case, it is possible that functionalization, which propitiates defects, may favor the bending of the sheets. Even in the area with more contrast, the ED of fh-BN still shows several six-fold symmetry patterns (Figure 6e), which may not only be due to stacking, but to the folding of the sheets as well. Nonetheless, it is certainly noticeable that less stacked boron nitride nanosheets can be obtained from the functionalized material. Additionally, we performed high-resolution TEM on h-BN and fh-BN sheets (Figure S6). Here we could see that the number of lattice fringes on the pristine h-BN sheets are more abundant and easier to find than in fh-BN sheets, which is consistent with a more stacked topology in pristine h-BN and support the observations in Figures 5b and 6.

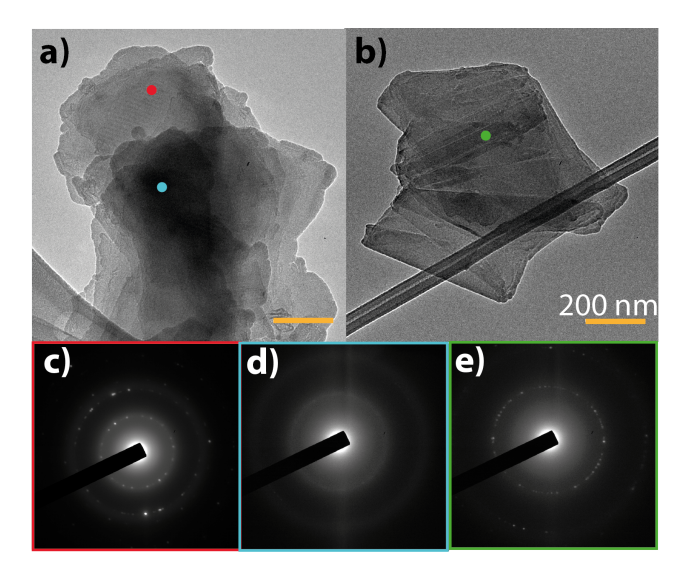


Figure 6. TEM images of h-BN (a) and fh-BN (b). Electron diffraction (ED) patterns for h-BN (c-d) and fh-BN (e).

SEM images were obtained by drop-casting the same kind of dispersion but centrifuged at a lower speed (1000g) in order to obtain larger sheets for analysis. It would be difficult to observe the features of smaller, thinner sheets, as the sample is covered with a 2 nm gold coating. The images presented corroborate a few of the characteristics seen in the TEM. For example, the stacking of hexagonal boron nitride sheets is prominent (Figure 7a), and it is difficult to discern the length of the individual sheets. In contrast, the fh-BN flake observed in Figure 7b does not seem to be stacked in as many layers as h-BN. Similarly to the TEM images, the edges on h-BN seem softer and rounder when compared to fh-BN flakes, which appear pointier and suggest some kind of cutting.

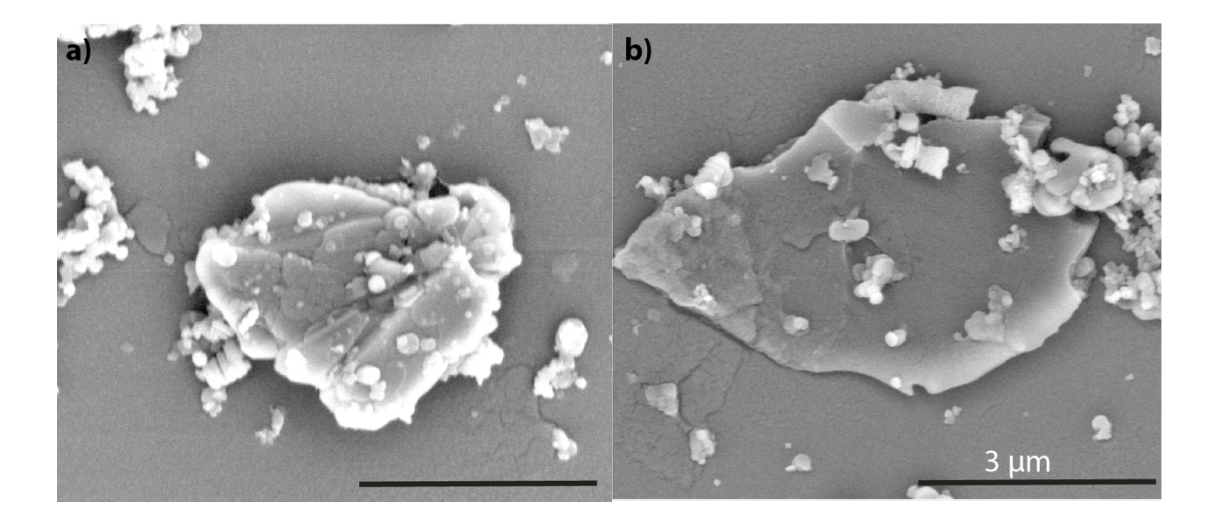


Figure 7. SEM images of (a) h-BN and (b) fh-BN drop-casted from a 1,000g-centrifuged IPA dispersion.

Defunctionalization. For functionalized BNNTs we previously demonstrated that we can selectively remove the hydrophobic chains to regenerate non-functionalized material. This is thanks to the high thermal stability of the h-BN material. The defunctionalization reaction was performed by slowly ramping the temperature to 650 °C (10 °C per minute) of a sample of fh-BN under argon, after which an 8.5 % in weigh is loss is observed (Figure S7a, red curve). This weight loss is due to the detachment of aliphatic chains. The sample is allowed to cool down and another temperature ramp is applied showing no weight loss, which is consistent with the absence of aliphatic groups in h-BN (Figure S7a, blue curve). Characterization of the defunctionalized material using FTIR shows that the C-H stretching bands in the area of 2780-3020 cm⁻¹ are absent in contrast with the fh-BN material before the thermal defunctionalization reaction (Figure S7b). This implies that fh-BN can be safely defunctionalized to recover pristine h-BN, which has important implications for the manufacture of boron-nitride materials and composites.

Hydrophobic films made of alkylated white graphene. We prepared a film by filtrating IPA dispersions of h-BN and fh-BN through hydrophilic nylon films and analyzed their affinity to water using water contact angle measurements. When measurements were performed on the h-BN film, the water drop would immediately collapse and spread on the film (Figure 8a). In contrast, the water drop would stay on top of the fh-BN film for long periods of time (Figure 8b), indicative of a more hydrophobic surface, which is consistent with the dispersibility results in water (Figure 4). The water contact angle was measured at three different spots of the film and averaged. The value obtained of 141.0° (±0.9) obtained for fh-BN is significantly greater than the value of 12.5° (±1.6) calculated for h-BN. According to such values, the h-BN film is considered hydrophilic, whereas the fh-BN film is considered hydrophobic, bordering on superhydrophobic (>150°).62 Figure 8c demonstrates how a film of fh-BN could serve as a coating for surfaces. A water drop was placed on fh-BN and on the nylon edge. While the nylon drop collapsed within 5 seconds, the drop on the fh-BN film lasted indefinitely. Finally, the same film was placed on top of a white LED to show that it is relatively transparent in addition to being repellent to water (Figure 8d-e).

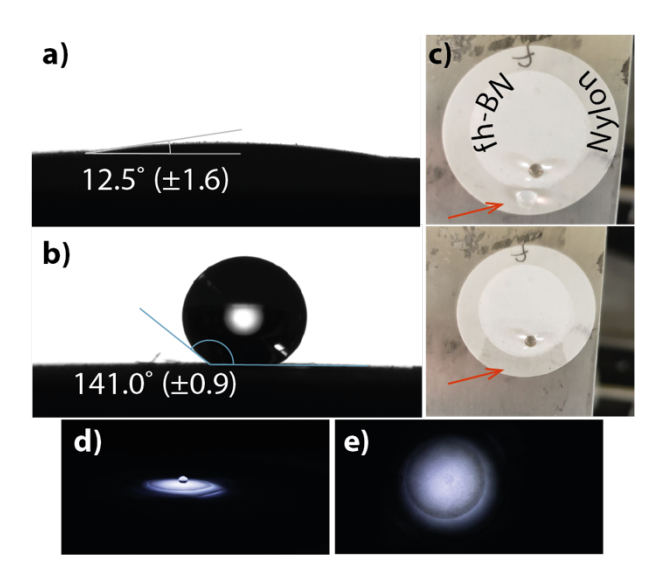


Figure 8. Water contact angle measurements of h-BN (a) and fh-BN (b) films prepared on nylon. (c) The water droplet stays still on fh-BN but collapses on the nylon surface in less than 5 seconds. (d) front and (e) top views of the fh-BN film with a water droplet on top and illuminated from below with an LED.

CONCLUSIONS

In summary, we utilized the Billups-Birch reaction to alkylate hexagonal boron nitride using 1-bromododecane and lithium as reagents. We demonstrate that functionalization of hexagonal boron nitride using this kind of reaction is tunable and reproducible. Using FTIR and TGA as complementary tools to assess the degree of functionalization, we determined that the highest degree of functionalization can be obtained when using a boron nitride to lithium ratio of 1:20. Such results were also indicated by XPS. This ratio likely provides enough lithium to outweigh side reactions with ammonia but using more than 20 equivalents may incite alkyl radicals side reactions. The alkyl decoration of boron nitride grants the sheets with different dispersibility behavior. While functionalization results in a material with an affinity to dodecane, a non-polar solvent, the contrary occurs when dispersed in water. Using AFM, we observed that dispersions of IPA are composed of a few layers of fh-BN sheets while dispersions of h-BN in the same solvent

present high agglomerations of sheets. Structural characterization with TEM and SEM revealed

that fh-BN appears with sharper edges and less stacked than h-BN. We found also that the aliphatic

functional groups in fh-BN can be safely removed by a thermal treatment. Finally, we prepared

films with h-BN and fh-BN 1:20 to study their affinity to water droplets. While the angle of water

in contact with the h-BN film indicates a hydrophilic surface, the angle on fh-BN is characteristic

of a very hydrophobic surface. In the past, we showed that the Billups-Birch reaction is a

straightforward chemical tool to functionalize BNNTs and in this work we demonstrate the

tunability of this reaction with their 2D analogs. We envision that if a stoichiometric study like

this were conducted with BNNTs, we would be able to find an even greater functionalization than

with h-BN, given the enhanced reactivity of nanotubes over sheets. However, given our experience

with both functionalized systems, we found that they have comparable properties regarding solvent

hydrophobicity, solvent dispersibility and ability to exfoliate better than their respective

precursors. We envision that alkyl-decorated boron nitride sheets provide a convenient material

that could serve for the fabrication of transparent coatings where repelling water is desired, such

as antifouling applications, as well as enhanced compatibility with polymers to produce

composites.

AUTHOR INFORMATION

Corresponding Author

Email: amarti@rice.edu

Author Contributions

23

The manuscript was written through contributions of all authors. All authors have given approval to the final version of the manuscript.

SUPPORTING INFORMATION

Typical FTIR spectra of h-BN and fh-BN, survey and high-resolution XPS, XPS data table, UV-Vis spectra and absolute values at 255 nm, high-resolution TEM, and defunctionalization characterization (FTIR and TGA).

ACKNOWLEDGMENT

We acknowledge the National Science Foundation (CHE-1807737) and AFOSR (FA9550-18-1-0014) for financial support. M.P. acknowledges the financial support of the Welch foundation (C-1668).

REFERENCES

- 1. Novoselov, K. S.; Geim, A. K.; Morozov, S. V.; Jiang, D.; Zhang, Y.; Dubonos, S. V.; Grigorieva, I. V.; Firsov, A. A. Electric Field Effect in Atomically Thin Carbon Films. *Science* **2004**, *306*, 666-669.
- 2. Iijima, S.; Ichihashi, T. Single-Shell Carbon Nanotubes of 1-nm Diameter. *Nature* **1993**, *363*, 603-605.
- 3. Kroto, H. W.; Heath, J. R.; O'Brien, S. C.; Curl, R. F.; Smalley, R. E. C_{∞}: Buckminsterfullerene. *Nature* **1985**, *318*, 162-163.
- 4. Novoselov, K. S.; Jiang, D.; Schedin, F.; Booth, T. J.; Khotkevich, V. V.; Morozov, S. V.; Geim, A. K. Two-Dimensional Atomic Crystals. *Proc. Natl. Acad. Sci.* **2005**, *102*, 10451-10453.
- 5. Liu, H.; Neal, A. T.; Zhu, Z.; Luo, Z.; Xu, X.; Tománek, D.; Ye, P. D. Phosphorene: An Unexplored 2D Semiconductor with a High Hole Mobility. *ACS Nano* **2014**, *8*, 4033-4041.
- 6. Puthirath Balan, A.; Radhakrishnan, S.; Woellner, C. F.; Sinha, S. K.; Deng, L.; de los Reyes, C. A.; Rao, B. M.; Paulose, M.; Neupane, R.; Apte, A., *et al.* Exfoliation of a Non-Van Der Waals Material from Iron Ore Hematite. *Nature Nanotechnol.* **2018**, *13*, 602-609.
- 7. Coleman, J. N.; Lotya, M.; O'Neill, A.; Bergin, S. D.; King, P. J.; Khan, U.; Young, K.; Gaucher, A.; De, S.; Smith, R. J., *et al.* Two-Dimensional Nanosheets Produced by Liquid Exfoliation of Layered Materials. *Science* **2011**, *331*, 568-571.

- 8. Falin, A.; Cai, Q.; Santos, E. J. G.; Scullion, D.; Qian, D.; Zhang, R.; Yang, Z.; Huang, S.; Watanabe, K.; Taniguchi, T., *et al.* Mechanical Properties of Atomically Thin Boron Nitride and the Role of Interlayer Interactions. *Nat. Commun.* **2017**, *8*, 15815.
- 9. Jo, I.; Pettes, M. T.; Kim, J.; Watanabe, K.; Taniguchi, T.; Yao, Z.; Shi, L. Thermal Conductivity and Phonon Transport in Suspended Few-Layer Hexagonal Boron Nitride. *Nano Lett.* **2013**, *13*, 550-554.
- 10. Ho, C. Y.; Powell, R. W.; Liley, P. E. Thermal Conductivity of the Elements. *J. Phys. Chem. Ref. Data* **1972**, *1*, 279-421.
- 11. Watanabe, K.; Taniguchi, T.; Kanda, H. Direct-Bandgap Properties and Evidence for Ultraviolet Lasing of Hexagonal Boron Nitride Single Crystal. *Nat. Mater.* **2004**, *3*, 404-409.
- 12. Zhu, J.; Kang, J.; Kang, J.; Jariwala, D.; Wood, J. D.; Seo, J.-W. T.; Chen, K.-S.; Marks, T. J.; Hersam, M. C. Solution-Processed Dielectrics Based on Thickness-Sorted Two-Dimensional Hexagonal Boron Nitride Nanosheets. *Nano Lett.* **2015**, *15*, 7029-7036.
- 13. Bresnehan, M. S.; Hollander, M. J.; Wetherington, M.; Wang, K.; Miyagi, T.; Pastir, G.; Snyder, D. W.; Gengler, J. J.; Voevodin, A. A.; Mitchel, W. C., *et al.* Prospects of Direct Growth Boron Nitride Films as Substrates for Graphene Electronics. *J. Mater. Res.* **2014**, *29*, 459-471.
- 14. Tran, T. T.; Bray, K.; Ford, M. J.; Toth, M.; Aharonovich, I. Quantum Emission from Hexagonal Boron Nitride Monolayers. *Nature Nanotechnol.* **2015**, *11*, 37-41.
- 15. Doan, T. C.; Majety, S.; Grenadier, S.; Li, J.; Lin, J. Y.; Jiang, H. X. Fabrication and Characterization of Solid-State Thermal Neutron Detectors Based on Hexagonal Boron Nitride Epilayers. *Nucl. Instrum. Methods Phys. Res. A* **2014**, *748*, 84-90.
- 16. Doan, T. C.; Li, J.; Lin, J. Y.; Jiang, H. X. Growth and Device Processing of Hexagonal Boron Nitride Epilayers for Thermal Neutron and Deep Ultraviolet Detectors. *AIP Adv.* **2016**, *6*, 075213.
- 17. Cai, Q.; Mateti, S.; Watanabe, K.; Taniguchi, T.; Huang, S.; Chen, Y.; Li, L. H. Boron Nitride Nanosheet-Veiled Gold Nanoparticles for Surface-Enhanced Raman Scattering. *ACS Appl. Mater. Interfaces* **2016**, *8*, 15630-15636.
- 18. Nurunnabi, M.; Nafiujjaman, M.; Lee, S.-J.; Park, I.-K.; Huh, K. M.; Lee, Y.-k. Preparation of Ultra-Thin Hexagonal Boron Nitride Nanoplates for Cancer Cell Imaging and Neurotransmitter Sensing. *Chem. Commun.* **2016**, *52*, 6146-6149.
- 19. Li, L. H.; Cervenka, J.; Watanabe, K.; Taniguchi, T.; Chen, Y. Strong Oxidation Resistance of Atomically Thin Boron Nitride Nanosheets. *ACS Nano* **2014**, *8*, 1457-1462.
- 20. Zhi, C.; Bando, Y.; Tang, C.; Kuwahara, H.; Golberg, D. Large-Scale Fabrication of Boron Nitride Nanosheets and Their Utilization in Polymeric Composites with Improved Thermal and Mechanical Properties. *Adv. Mater.* **2009**, *21*, 2889-2893.
- 21. Lin, Z.; McNamara, A.; Liu, Y.; Moon, K.-s.; Wong, C.-P. Exfoliated Hexagonal Boron Nitride-Based Polymer Nanocomposite with Enhanced Thermal Conductivity for Electronic Encapsulation. *Compos. Sci. Technol.* **2014**, *90*, 123-128.
- 22. Boland, C. S.; Barwich, S.; Khan, U.; Coleman, J. N. High Stiffness Nano-Composite Fibres from Polyvinylalcohol Filled with Graphene and Boron Nitride. *Carbon* **2016**, *99*, 280-288.
- 23. Taha-Tijerina, J.; Narayanan, T. N.; Gao, G.; Rohde, M.; Tsentalovich, D. A.; Pasquali, M.; Ajayan, P. M. Electrically Insulating Thermal Nano-Oils Using 2D Fillers. *ACS Nano* **2012**, *6*, 1214-1220.

- 24. Lin, Y.; Williams, T. V.; Xu, T.-B.; Cao, W.; Elsayed-Ali, H. E.; Connell, J. W. Aqueous Dispersions of Few-Layered and Monolayered Hexagonal Boron Nitride Nanosheets from Sonication-Assisted Hydrolysis: Critical Role of Water. *J. Phys. Chem. C* **2011**, *115*, 2679-2685.
- 25. Liao, Y.; Chen, Z.; Connell, J. W.; Fay, C. C.; Park, C.; Kim, J.-W.; Lin, Y. Chemical Sharpening, Shortening, and Unzipping of Boron Nitride Nanotubes. *Adv. Funct. Mater.* **2014**, 24, 4497-4506.
- 26. Sainsbury, T.; O'Neill, A.; Passarelli, M. K.; Seraffon, M.; Gohil, D.; Gnaniah, S.; Spencer, S. J.; Rae, A.; Coleman, J. N. Dibromocarbene Functionalization of Boron Nitride Nanosheets: Toward Band Gap Manipulation and Nanocomposite Applications. *Chem. Mater.* **2014**, *26*, 7039-7050.
- 27. Zhi, C. Y.; Bando, Y.; Terao, T.; Tang, C. C.; Kuwahara, H.; Golberg, D. Chemically Activated Boron Nitride Nanotubes. *Chemistry An Asian Journal* **2009**, *4*, 1536-1540.
- 28. Xiao, F.; Naficy, S.; Casillas, G.; Khan, M. H.; Katkus, T.; Jiang, L.; Liu, H.; Li, H.; Huang, Z. Edge-Hydroxylated Boron Nitride Nanosheets as an Effective Additive to Improve the Thermal Response of Hydrogels. *Adv. Mater.* **2015**, *27*, 7196-7203.
- 29. Sainsbury, T.; Satti, A.; May, P.; Wang, Z.; McGovern, I.; Gun'ko, Y. K.; Coleman, J. Oxygen Radical Functionalization of Boron Nitride Nanosheets. *J. Am. Chem. Soc.* **2012**, *134*, 18758-18771.
- 30. Pakdel, A.; Bando, Y.; Golberg, D. Plasma-Assisted Interface Engineering of Boron Nitride Nanostructure Films. *ACS Nano* **2014**, *8*, 10631-10639.
- 31. Ikuno, T.; Sainsbury, T.; Okawa, D.; Fréchet, J. M. J.; Zettl, A. Amine-Functionalized Boron Nitride Nanotubes. *Solid State Commun.* **2007**, *142*, 643-646.
- 32. Lee, D.; Lee, B.; Park, K. H.; Ryu, H. J.; Jeon, S.; Hong, S. H. Scalable Exfoliation Process for Highly Soluble Boron Nitride Nanoplatelets by Hydroxide-Assisted Ball Milling. *Nano Lett.* **2015**, *15*, 1238-1244.
- 33. Lei, W.; Mochalin, V. N.; Liu, D.; Qin, S.; Gogotsi, Y.; Chen, Y. Boron Nitride Colloidal Solutions, Ultralight Aerogels and Freestanding Membranes through One-Step Exfoliation and Functionalization. *Nat. Commun.* **2015**, *6*, 8849.
- 34. He, M.; Swager, T. M. Covalent Functionalization of Carbon Nanomaterials with Iodonium Salts. *Chem. Mater.* **2016**, *28*, 8542-8549.
- 35. Maeda, Y.; Takehana, Y.; Dang, J.-S.; Suzuki, M.; Yamada, M.; Nagase, S. Effect of Substituents and Initial Degree of Functionalization of Alkylated Single-Walled Carbon Nanotubes on Their Thermal Stability and Photoluminescence Properties. *Chem. Eur. J.* **2017**, 23, 1789-1794.
- 36. Martinez-Rubi, Y.; Guan, J.; Lin, S.; Scriver, C.; Sturgeon, R. E.; Simard, B. Rapid and Controllable Covalent Functionalization of Single-Walled Carbon Nanotubes at Room Temperature. *Chem. Commun.* **2007**, 5146-5148.
- 37. Voiry, D.; Roubeau, O.; Penicaud, A. Stoichiometric Control of Single Walled Carbon Nanotubes Functionalization. *J. Mater. Chem.* **2010**, *20*, 4385-4391.
- 38. Shin, H.; Guan, J.; Zgierski, M. Z.; Kim, K. S.; Kingston, C. T.; Simard, B. Covalent Functionalization of Boron Nitride Nanotubes via Reduction Chemistry. *ACS Nano* **2015**, *9*, 12573-12582.
- 39. Chakraborty, S.; Chattopadhyay, J.; Guo, W.; Billups, W. E. Functionalization of Potassium Graphite. *Angew. Chem.* **2007**, *119*, 4570-4572.

- 40. Chen, Y.; Haddon, R. C.; Fang, S.; Rao, A. M.; Eklund, P. C.; Lee, W. H.; Dickey, E. C.; Grulke, E. A.; Pendergrass, J. C.; Chavan, A., *et al.* Chemical Attachment of Organic Functional Groups to Single-Walled Carbon Nanotube Material. *J. Mater. Res.* **1998**, *13*, 2423-2431.
- 41. Pekker, S.; Salvetat, J.-P.; Jakab, E.; Bonard, J.-M.; Forró, L. Hydrogenation of Carbon Nanotubes and Graphite in Liquid Ammonia. *J. Phys. Chem. B* **2001**, *105*, 7938-7943.
- 42. Haufler, R. E.; Conceicao, J.; Chibante, L. P. F.; Chai, Y.; Byrne, N. E.; Flanagan, S.; Haley, M. M.; O'Brien, S. C.; Pan, C.; Xiao, Z., *et al.* Efficient Production of C_∞ (Buckminsterfullerene), C_∞H_∞, and the Solvated Buckide Ion. *J. Phys. Chem.* **1990**, *94*, 8634-8636.
- 43. Chattopadhyay, J.; Sadana, A. K.; Liang, F.; Beach, J. M.; Xiao, Y.; Hauge, R. H.; Billups, W. E. Carbon Nanotube Salts. Arylation of Single-Wall Carbon Nanotubes. *Org. Lett.* **2005**, *7*, 4067-4069.
- 44. Liang, F.; Sadana, A. K.; Peera, A.; Chattopadhyay, J.; Gu, Z.; Hauge, R. H.; Billups, W. E. A Convenient Route to Functionalized Carbon Nanotubes. *Nano Lett.* **2004**, *4*, 1257-1260.
- 45. Liang, F.; Alemany, L. B.; Beach, J. M.; Billups, W. E. Structure Analyses of Dodecylated Single-Walled Carbon Nanotubes. *J. Am. Chem. Soc.* **2005**, *127*, 13941-13948.
- 46. Ghosh, S.; Wei, F.; Bachilo, S. M.; Hauge, R. H.; Billups, W. E.; Weisman, R. B. Structure-Dependent Thermal Defunctionalization of Single-Walled Carbon Nanotubes. *ACS Nano* **2015**, *9*, 6324-6332.
- 47. Wunderlich, D.; Hauke, F.; Hirsch, A. Preferred Functionalization of Metallic and Small-Diameter Single Walled Carbon Nanotubes Via Reductive Alkylation. *J. Mater. Chem.* **2008**, *18*, 1493-1497.
- 48. Gebhardt, B.; Syrgiannis, Z.; Backes, C.; Graupner, R.; Hauke, F.; Hirsch, A. Carbon Nanotube Sidewall Functionalization with Carbonyl Compounds—Modified Birch Conditions Vs the Organometallic Reduction Approach. *J. Am. Chem. Soc.* **2011**, *133*, 7985-7995.
- 49. Chakraborty, S.; Guo, W.; Hauge, R. H.; Billups, W. E. Reductive Alkylation of Fluorinated Graphite. *Chem. Mater.* **2008**, *20*, 3134-3136.
- 50. de los Reyes, C. A.; Walz Mitra, K. L.; Smith, A. D.; Yazdi, S.; Loredo, A.; Frankovsky, F. J.; Ringe, E.; Pasquali, M.; Martí, A. A. Chemical Decoration of Boron Nitride Nanotubes Using the Billups-Birch Reaction: Toward Enhanced Thermostable Reinforced Polymer and Ceramic Nanocomposites. *ACS Appl. Nano Mat.* **2018**, *1*, 2421-2429.
- 51. de los Reyes, C. A.; Smith McWilliams, A. D.; Hernández, K.; Walz-Mitra, K. L.; Ergülen, S.; Pasquali, M.; Martí, A. A. Adverse Effect of Ptfe Stir Bars on the Covalent Functionalization of Carbon and Boron Nitride Nanotubes Using Billups–Birch Reduction Conditions. *ACS Omega* **2019**, *4*, 5098-5106.
- 52. Chattopadhyay, J.; Chakraborty, S.; Mukherjee, A.; Wang, R.; Engel, P. S.; Billups, W. E. Set Mechanism in the Functionalization of Single-Walled Carbon Nanotubes. *J. Phys. Chem. C* **2007**, *111*, 17928-17932.
- 53. Shi, Y.; Hamsen, C.; Jia, X.; Kim, K. K.; Reina, A.; Hofmann, M.; Hsu, A. L.; Zhang, K.; Li, H.; Juang, Z.-Y., *et al.* Synthesis of Few-Layer Hexagonal Boron Nitride Thin Film by Chemical Vapor Deposition. *Nano Lett.* **2010**, *10*, 4134-4139.
- 54. Bergstrom, F. W.; Fernelius, W. C. The Chemistry of the Alkali Amides. *Chem. Rev.* **1933**, *12*, 43-179.
- 55. Zhang, K. S.; Pham, D.; Lawal, O.; Ghosh, S.; Gangoli, V. S.; Smalley, P.; Kennedy, K.; Brinson, B. E.; Billups, W. E.; Hauge, R. H., *et al.* Overcoming Catalyst Residue Inhibition of

- the Functionalization of Single-Walled Carbon Nanotubes Via the Billups–Birch Reduction. *ACS Appl. Mater. Interfaces* **2017**, *9*, 37972-37980.
- 56. Pham, D.; Zhang, S. K.; Lawal, O.; Ghosh, S.; Gangoli, S. V.; Ainscough, J. T.; Kellogg, B.; Hauge, H. R.; Adams, W. W.; Barron, R. A. Apparatus for Scalable Functionalization of Single-Walled Carbon Nanotubes Via the Billups-Birch Reduction. *C* **2017**, *3*.
- 57. Henck, H.; Pierucci, D.; Fugallo, G.; Avila, J.; Cassabois, G.; Dappe, Y. J.; Silly, M. G.; Chen, C.; Gil, B.; Gatti, M., *et al.* Direct Observation of the Band Structure in Bulk Hexagonal Boron Nitride. *Phys. Rev. B* **2017**, *95*, 085410.
- 58. Wang, Y.; Trenary, M. Surface Chemistry of Boron Oxidation. 2. The Reactions of Boron Oxides B₂O₂ and B₂O₃ with Boron Films Grown on Tantalum(110). *Chem. Mater.* **1993**, *5*, 199-205.
- 59. Wan, S.; Yu, Y.; Pu, J.; Lu, Z. Facile Fabrication of Boron Nitride Nanosheets-Amorphous Carbon Hybrid Film for Optoelectronic Applications. *RSC Adv.* **2015**, *5*, 19236-19240.
- 60. Meyer, J. C.; Geim, A. K.; Katsnelson, M. I.; Novoselov, K. S.; Booth, T. J.; Roth, S. The Structure of Suspended Graphene Sheets. *Nature* **2007**, *446*, 60-63.
- 61. Li, L. H.; Chen, Y.; Behan, G.; Zhang, H.; Petravic, M.; Glushenkov, A. M. Large-Scale Mechanical Peeling of Boron Nitride Nanosheets by Low-Energy Ball Milling. *J. Mater. Chem.* **2011**, *21*, 11862-11866.
- 62. Nuraje, N.; Khan, W. S.; Lei, Y.; Ceylan, M.; Asmatulu, R. Superhydrophobic Electrospun Nanofibers. *J. Mater. Chem. A* **2013**, *1*, 1929-1946.

TOC Graphic:

